Journal of Power Sources 455 (2020) 227973

Contents lists available at ScienceDirect

Journal of Power Sources

journal homepage: www.elsevier.com/locate/jpowsour

B_2H_6 splitting on catalytic surfaces and role of BH_3 towards hydrogen spillover

E.S. Erakulan [a,1], E. Mathan Kumar [b,1], Puru Jena [c], Ranjit Thapa [a,*]

[a] Department of Physics, SRM University, Amaravati, 522 502, Andhra Pradesh, India
[b] SRM Research Institute, SRM Institute of Science and Technology, Kattankulathur, 603203, Tamil Nadu, India
[c] Department of Physics, Virginia Commonwealth University, Richmond, VA, 23284, USA

HIGHLIGHTS

- A predictive model equation is proposed to estimate the binding energy of BH_3 molecule/s.
- Design the active surfaces to split the B_2H_6 into two BH_3 molecules.
- BH_3 is found to be universal secondary catalyst for bond exchange hydrogen spillover mechanism. .

GRAPHICAL ABSTRACT

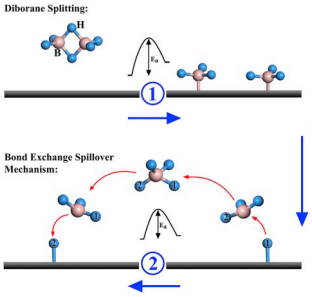

ARTICLE INFO

Keywords:
Hydrogen storage
Adsorption
Catalyst
Descriptor
Density functional theory
Predictive model equation

ABSTRACT

A fundamental understanding of the spillover mechanism is an open and challenging problem and plays an important role in catalysis. In particular, bond-exchange spillover mechanism is considered to be effective for reversible storage and release of hydrogen at near ambient conditions. For this, three critical steps are needed: finding the right support (acceptor), the right catalyst to split H_2, and ensuring that once H_2 is split, the H atoms can migrate on the surface with the help of secondary catalysts and eventually hydrogenate the entire material. In this paper we address these challenges using density functional theory. We show that BH_3, a secondary catalyst, can be produced by symmetrically splitting its stable precursor, B_2H_6, on doped metal-free surfaces such as graphene and h-BN as well as on MOF5. In addition, to reduce computational cost, we develop structural descriptor and predictive model equation to effectively screen potential BH_3 binding sites. Symmetrical splitting of B_2H_6 on different types of materials can address the hydrogen spillover challenge, making efficient storage of hydrogen possible.

1. Introduction

Hydrogen can be used as a clean alternative to fossil fuels only if many challenges in its production, storage, and use in fuel cells can be overcome. Among these, the greatest challenge is to find ways to store hydrogen safely and efficiently under ambient conditions, with high

* Corresponding author.
E-mail address: ranjit.phy@gmail.com (R. Thapa).
[1] Same contributed first author.

https://doi.org/10.1016/j.jpowsour.2020.227973
Received 21 January 2020; Accepted 26 February 2020
Available online 4 March 2020

gravimetric and volumetric density [1,2]. While hydrogen is currently stored in automobiles in high pressure tanks or in liquid form, it is not ideal for widespread commercial use. Considerable research has been carried out to identify light-weight materials that can store hydrogen to meet industry requirements [3–7]. In this connection, hydrogen spill over mechanism has been shown to be useful because the first step in the hydrogen storage process is to split H_2 molecules so that the hydrogen atoms can diffuse through the material and stay bound [8–11]. However, splitting hydrogen would require high temperature, which can induce thermodynamic instability in the host materials [12–14]. Thus, secondary catalysts are needed to achieve H atom diffusion, without compromising the stability of the host material. Consequently, works [15–18] have focused on studies of hydrogen spillover mechanism and the role of secondary catalysts supported on different surfaces.

In a theoretical work, Li et al. [19], aimed to achieve high hydrogen storage capacity in metal organic frameworks (MOFs) by introducing a bridge-building technique, which promotes the H spillover process. Under room temperature and 10 MPa pressure, reversible hydrogen storage capacity of 4 wt% was achieved in bridged IRMOF-8. Han et al. [20], using DFT, observed that the polar hydride molecules (shuttle gas) such as NH_3, HF and H_2O can provide a favorable thermodynamic and catalytic effect for reducing the migration barrier on the graphene surface. Similarly, it has been shown through DFT that h-BN and SiC monolayers can be hydrogenated via bond-exchange spillover mechanism with low H migration barrier energy [21,22]. Secondary catalysts (external mediators) such as borane (BH_3), gallane (GaH_3), ammonia (NH_3) and silane (SiH_4) were tested for bond-exchange spillover andit was found that only BH_3 and GaH_3 were suitable for h-BN and SiC surface. However, these two monomers are unstable and more reactive compared to their oligomers.

Thus, generating a monomer from its stable oligomer using active catalysts is an important step to achieve a hydrogenated surface. In a recent First-principles work, Park et al., reported the possible dissociation of B_2H_6 into two BH_3 molecules on TiN (001) surface with a small energy barrier of 1.11 eV [23]. The splitting of B_2H_6 is also necessary for the formation of borohydrides such as $LiBH_4$, whose decomposition again results in diborane [24]. Tuning of this cyclic process is proposed to be a reversible hydrogen sorption reaction for hydrogen storage. Another study by Parry, where di-borane reaction with bases were studied, found that, whether the splitting of B_2H_6 is symmetric or asymmetric would depend on the dielectric constant of the base [25]. Also, reactions of B_2H_6 with ammonia has been studied in detail both experimentally and theoretically, where the first step involves cleavage and formation of an adduct with ammonia and the second step involves H_2 release [26–29].

In this work, using density functional theory, we study the symmetrical splitting of B_2H_6 to generate BH_3 on metal-free surfaces and MOF5. Using the binding energy and energy barrier calculations, we have also developed a structural descriptor and a predictive model equation that provides a comprehensive road map to implement the bond-exchange spillover of hydrogen on graphene. We have considered N-doped graphene as well as O- and C-doped h-BN. On h-BN surface, two different doping levels were studied - two oxygen atoms at two next-nearest neighbor N sites and three carbon atoms doped at three consecutive B sites (see Fig. 1 (b)). Both doping levels are found to be sufficient to split B_2H_6 symmetrically, irrespective of their arrangements. Using the structural descriptor, we can find, without excessive computational cost, the suitable N-doped graphene surface capable of splitting B_2H_6. In addition, we discuss the migration of H on N-doped graphene surface using the secondary catalyst. Finally, the validity of bond exchange spillover mechanism and di-borane splitting has been tested on MOF5.

2. Computational details

The calculations are performed using spin polarized density

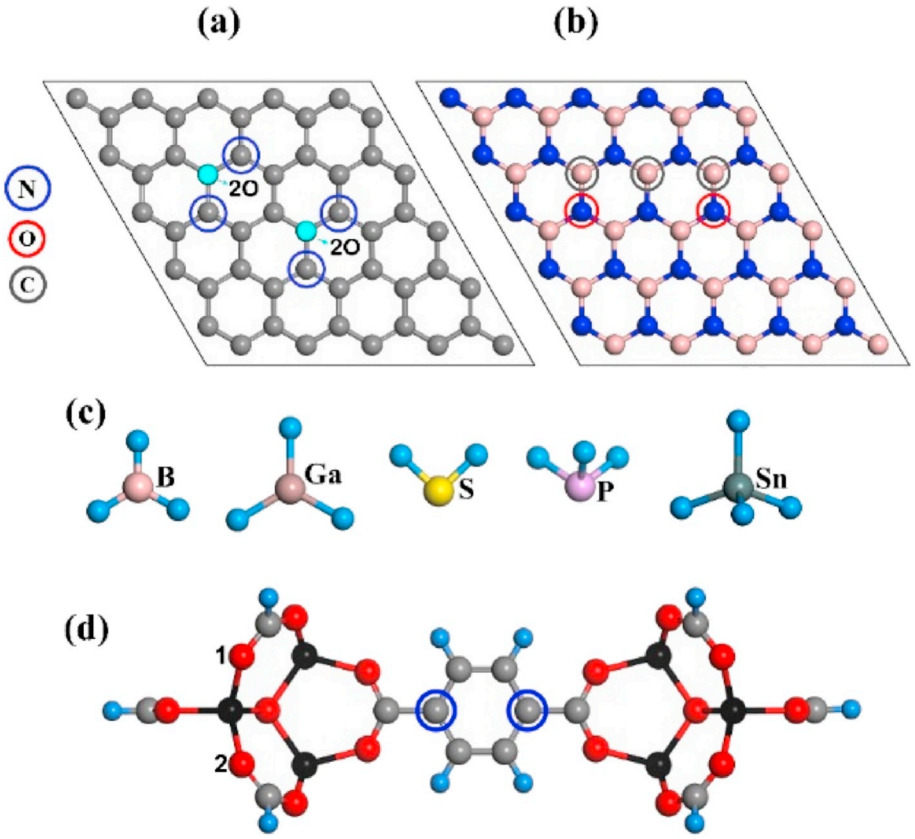

Fig. 1. (a) 5x5 supercell of graphene with N-dopant sites marked by blue circles. This configuration is termed as 2O representing the C atom at the Ortho site with respect to the N-dopants. (b) 5x5 supercell of h-BN surface. The grey and red colored circles denote B sites replaced by C and N sites replaced by O, respectively. (c) Geometries of the hydride molecules BH_3, GaH_3, H_2S, PH_3, SnH_4. (d) MOF5 modeled by two metal-oxide clusters linked by Benzene di-carboxylate linker. Dangling bonds are terminated with hydrogen. Grey, red, black, blue and light blue spheres denote carbon, oxygen, zinc, nitrogen and hydrogen atoms. (For interpretation of the references to color in this figure legend, the reader is referred to the Web version of this article.)

functional theory as implemented in the Vienna ab-initio simulation package (VASP) [30]. The exchange and correlation potential is treated using the generalized gradient approximation (GGA) due to Perdew–Burke–Ernzerhof (PBE) [31]. The potentials of the atoms are described by the projected augmented wave (PAW) method [32]. The plane-wave basis set is considered with an energy cut-off of 500 eV. Brillouin zone is sampled using the Monkhorst Pack scheme with a $5 \times 5 \times 1$ K-point grid for monolayers and $2 \times 2 \times 2$ K-point grid for MOF5. All structures are optimized until the total energy and the maximum force converged to less than 10^{-4} eV per atom and 0.001 eV $Å^{-1}$, respectively. Henkleman's Bader Charge analysis is used to study the accumulation or depletion of charge in a given system [33]. The climbing nudged elastic band (c-NEB) method is used to locate the saddle point [34]. In addition to DFT calculations, KMC method implemented in Material Studio can also be employed to study the reaction mechanisms [35]. We used 5x5 supercell and 15 Å vacuum space along the c-axis to simulate the 2D surfaces. MOF5 is modeled with two metal oxide clusters linked by Benzene di-carboxylate (BDC) linker. Remaining ends in the metal oxide cluster are terminated with hydrogen atoms.

3. Results and discussion

Our first step is to identify the hydride molecule that could best serve as a secondary catalyst. Next, we determine the ways to split this precursor molecule to produce the required secondary catalyst. Then we study the role of adsorbed BH_3 in splitting the H_2 molecule. Finally, we study the migration of hydrogen by generalizing the bond-exchange spillover mechanism. For catalyst support we considered three different substrates – graphene, h-BN, and MOF5. In the following we discuss our results.

3.1. Identifying the preferred secondary catalyst

As pointed out earlier, BH_3 and GaH_3 were found to be good secondary catalysts to split the H_2 molecule on h-BN and SiC surface. Because both BH_3 and GaH_3 are unstable monomers and combine to form stable B_2H_6 and Ga_2H_6, respectively, we first study the binding of several other hydride gas molecules such as H_2S, PH_3, and SnH_4 on pure and doped graphene and hexagonal boron nitride (h-BN) monolayer to see if they are suitable as secondary catalysts. The structures of 2D graphene, h-BN, and a model representing MOF5 are shown in Fig. 1 (a), (b), and (d), respectively. The geometries of monomeric hydrides are shown in Fig. 1 (c). The sites where N atoms are doped in graphene and C and O atoms are doped in h-BN are marked in Fig. 1a and b, respectively. The binding energy of the hydride molecule is chosen as the determining factor in the search of suitable secondary catalyst molecule (binding energy should be near to the chemisorption range, ~1–10 eV, for bond-exchange spillover mechanism). Note that the secondary catalysts, bound weakly to the surface, are not suitable for bond exchange mechanism as more energy would be required to form an adduct or to bind with the adsorbed hydrogen atom. In addition, weakly bound hydride molecules cannot lower the energy barrier associated with the migration of hydrogen atom on the host surface.

The binding energy of a molecule to a surface is defined by

$$E_{B.E.} = E(\text{surface} + \text{molecule}) - E(\text{surface}) - E(\text{molecule})$$

where E(surface + molecule), E(surface), and E(molecule) are the total energies of the surface with molecules adsorbed on it, the surface, and the molecule, respectively. A negative value of $E_{B.E.}$ means that the gas molecule is bound to the surface. In Table 1 we list the calculated binding energies of the hydride molecules on pure and N-doped graphene as well as pure and C and O doped h-BN. In the case of N-doped graphene, we calculate the binding energy of the gas molecules attached to both N and nearest C site. In h-BN, the hydride molecule is attached to both B and N sites. In C doped h-BN, binding energies are calculated for hydride molecule attached to B, C, and N sites, while on O-doped h-BN B, O and N sites are studied. We see that, with exception of SnH_4 bound to B site in O-doped h-BN, the binding energies are small compared to those of BH_3 and GaH_3 on all surfaces. Thus, we do not consider H_2S, PH_3, and SnH_4 as preferred candidates for secondary catalysts. The binding energies of hydride molecules with h-BN surface (both pure and doped) are greater than that on graphene. The increased binding energy on doped h-BN can be attributed to the creation of localized states near the Fermi level. To be noted that during relaxation of BH_3 on O site of O-doped h-BN, the molecule drifted and settled on neighbouring B atom, repelling from the O atom. Likewise, on N site of O-doped h-BN, GaH_3 settled on B atom drifting away from the N atom. We also perform Bader charge analysis to study charge transfer between the molecules and the surface, quantitatively. The results are given in Table S1. Note that the charge transfers in the case of BH_3 and GaH_3 are more than other hydride molecules, consistent with the binding energy trend. Charge density difference is also calculated for BH_3 molecule on all possible sites of the surfaces and on B site of O-doped h-BN, it is calculated for other molecules as well (See Fig. S2). In all the cases the there is accumulation of charge between the molecule and the surface and charge on the active site is depleted.

Table 1
Binding energies of monomeric hydrides.

System	Site	Binding Energy (eV)				
		BH_3	GaH_3	H_2S	PH_3	SnH_4
Pure Graphene	–	−0.34	−0.43	−0.12	−0.09	−0.29
N-doped Graphene	On C	−0.35	−0.39	−0.09	−0.13	−0.29
	On N	−0.19	−0.28	−0.12	−0.13	−0.27
h-BN	On B	−0.24	−0.39	−0.13	−0.06	−0.25
	On N	−0.69	−0.52	−0.13	−0.11	−0.32
C_h-BN	On B	−0.65	−0.53	−0.20	−0.12	−0.28
	On C	−1.15	−0.91	−0.16	−0.15	−0.31
	On N	−0.77	−0.60	−0.15	−0.12	−0.31
O_h-BN	On B	−1.90	−1.48	−0.19	−0.32	−0.55
	On O	–	−0.83	−0.27	−0.42	−0.26
	On N	−0.62	–	−0.21	−0.26	−0.34

Further, a similar binding energy study is carried out for the monomeric hydrides interacting with a single H atom adsorbed on pure and doped surfaces (h-BN and graphene). The magnitude of this binding energy determines the ability of each molecule to desorb hydrogen atom from the surface. The increased binding energy between external catalyst and the chemisorbed hydrogen on surface may lead to the formation of a possible adduct (see Table S2). In the case of an H atom chemisorbed on pure and N-doped graphene, BH_3 (B.E. = −0.45 eV and −0.52 eV, respectively) shows stronger interaction than GaH_3 (B.E. = −0.25 eV and −0.29 eV, respectively). Also, for H atom adsorbed on C and O-doped h-BN, BH_3 (B.E. = −0.53 eV and −1.05 eV, respectively) shows stronger interaction than GaH_3 (B.E. = −0.10 eV and −0.69 eV, respectively). The binding in GaH_3 lies closer to physisorption range in most cases, indicating that it is not suitable as a universal secondary catalyst. Thus, we conclude that BH_3 is the only preferred secondary catalyst for the H-atom migration on both the surfaces. Thus, for the remaining studies, we focus on BH_3 as the preferred molecule for bond-exchange spillover study.

3.2. Splitting of B_2H_6, structural descriptor, and predictive model equation

Note that BH_3 is unstable and readily dimerizes to produce B_2H_6 [36, 37]. To produce BH_3, one must, therefore, start with the stable precursor B_2H_6 and find efficient ways to split it. B_2H_6 molecule is formed by two bridging and four terminal hydrogen atoms (see Fig. S1 in supplementary information). The bridging hydrogen atoms are bonded with the boron atom through 3-center 2-electron bonding (banana bond). The two boron atoms are sp3 hybridized, of which two orbitals are bonded

with terminal hydrogen. The remaining two orbitals of each boron atom has one empty and one filled orbital from the bridge hydrogen atom. Consequently, two sp3 orbitals from two boron atoms combine to form the two bridging (banana) bond. This bridge hydrogen bond is weaker than the terminal hydrogen bond and hence symmetrical splitting of B_2H_6 is more probable through breaking of the bridge hydrogen bonds. The splitting of B_2H_6 molecule into two BH_3 molecules would require high energy barrier of 2.28 eV (see Fig. S3), implying the need for a catalyst to split B_2H_6. Role of catalysts in splitting B_2H_6 is discussed further.

3.2.1. B_2H_6 splitting on graphene surface

To see if a single N atom doped on the graphene surface is sufficient to bind two BH_3 molecules, we placed them near the dopant atom and optimized the structure. After relaxation, one of the BH_3 molecules was bound on the N atom while the other drifted away. This led us to conclude that more than one N atom is required to bind them, once B_2H_6 molecule is cleaved.

To find the active carbon sites and the number of nitrogen dopants needed to anchor the two BH_3 molecules strongly, it is necessary to first identify active sites relative to the nitrogen atom. We illustrate these active C sites as 1, 2, 3-Ortho, 1, 2, 3-Meta, and 1, 2, 3-Para sites with reference to the N dopants (see Fig. 2). The nearest site from the dopant is identified as Ortho, the site that is next to the ortho position is Meta, and the site that is diagonally opposite to the dopant atom in the hexagonal ring is the Para site, respectively. When more than one dopant atom is used, the ortho/meta/para sites are numbered as 2O, 2 M, 2P and 3O, 3 M, 3P, as shown in Fig. 2a. We calculate the BH_3 binding energy on all the nine sites (see Table S3). The binding energies corresponding to Ortho, Meta and Para positions with respect to the number of dopants varies linearly with different intercepts and slopes (shown in Fig. 2b). From this plot we construct structural descriptor-based equations for Ortho, Meta and Para positioned sites, respectively, as,

$$y = 0.61–0.905x \text{ (Ortho)} \quad (1)$$

$$y = -0.293 - 0.065x \text{ (Meta)} \quad (2)$$

$$y = -0.06 - 0.27x \text{ (Para)} \quad (3)$$

Here y and x denote the binding energy of BH_3 and number of Ortho/Meta/Para position with respect to the dopant site. We see that the 3-Ortho/Meta/Para carbon site has higher affinity for binding than 2 and 1-Ortho/Meta/Para carbon site. Moreover, the Ortho site has higher binding energy than all other possible sites. Using the above three structural descriptor-based equations, we construct a model equation to predict BH_3 binding energy for other active sites,

$$\text{B.E. } (BH_3) = (-0.905n_O + 0.61)O + (-0.065n_M - 0.293)M + (-0.27n_P - 0.06)P \quad (4)$$

Here, n_O, n_M and n_P denote the number of Ortho, Meta and Para positions, which are created by N dopant atoms and O, M, P describe the Ortho, Meta and Para identifiers. For example, according to the predictive model equation a single BH_3 that lies on two Ortho positions, ($O = 1$ & $n_O = 2$; $M = P = 0$) would have a binding energy of −1.2 eV. DFT based calculations performed for this configuration yields the binding energy to be −1.09 eV, which is in good agreement with that predicted by the model equation. This agreement confirms that the structural descriptor discussed above can account for the preferred binding site. To get a better picture, we plot the BH_3 binding energy, estimated for different sites, using the predictive model equation and compare them with those calculated using DFT. The results in Fig. 2c show the fit to be good with $R^2 = 0.95$. Similarly, we estimated two BH_3 molecules bound to the dopant site with varying concentration and minimum three N atoms doped at different configurations (2Ortho-1Para, 2Meta-2Meta, 3Ortho-3Ortho, 3Ortho-2Para) (see Fig. S5(a)–(d)). We find that the binding of two BH_3 molecules also follows the prediction of the model equation and the estimated binding energies match well with that calculated using DFT. For example, the binding energy obtained using the model equation for 2Ortho-1Para configuration is −1.53 eV, which is close to the DFT calculated energy of −1.38 eV. The goodness of the fit

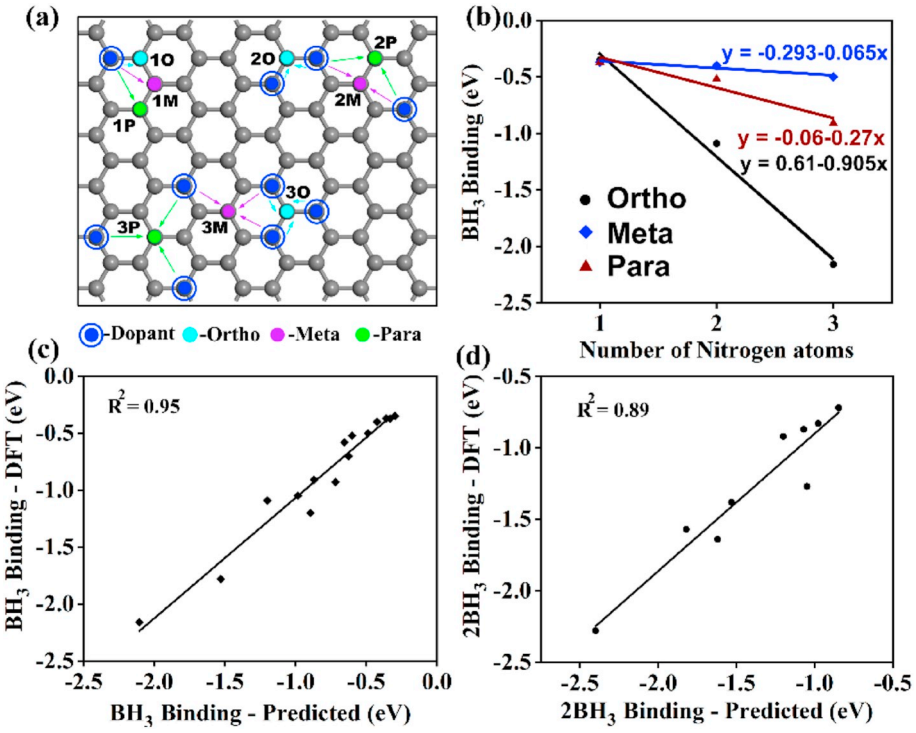

Fig. 2. (a) Model structure showing the 1,2,3 Ortho/Meta/Para carbon sites with respect to the dopant atoms. (b) Binding energy of BH_3 on carbon site corresponding to 1,2,3 Ortho, 1,2,3 Meta and 1,2,3 Para positions. Binding energy calculated using DFT vs. binding energy estimated using the predictive model equation for (c) single BH_3 molecule and (d) two BH_3 molecules.

in this case is found to be $R^2 = 0.89$ and the plot is shown in Fig. 2d. From the above analysis of binding energy, minimum four N dopant atoms are required to split the B_2H_6 and the structure must contain one 2- or 3-Ortho site and another 2-Ortho/Para/Meta site. We believe that our model equation is adequate to predict accurate binding sites and dopant concentration for BH_3 binding. This can reduce the computational effort of otherwise expensive DFT calculation.

From the above prediction, two sites with 2-Ortho configuration (4 N atoms as dopants), are considered for adsorption of two BH_3 molecules on graphene (see Fig. 1a). On 4N-doped graphene, the energy required to dissociate B_2H_6 into two BH_3 molecules is 0.77 eV, implying that BH_3 production is possible at ambient temperature (see Fig. 3a). In a recent work Zhang et al. use graphene as a support to anchor MgH_2 nanoparticles to produce $Mg(BH_4)_2$ by symmetrical splitting B_2H_6 on MgH_2 nanoparticles. The enthalpy of formation for $Mg(BH_4)_2$ is −308 kJ/mol [38].Nitrogen is also considered as a binding site and out of several configurations only one is found to be optimal (Figure S6 (a)). However, the barrier energy in this case is too high, indicating that nitrogen is not suitable as a site for B_2H_6 splitting (Figure S6 (b)). On the H-atom adsorbed on 3N-doped graphene surface, the B_2H_6 splitting barrier energy is 1.74 eV (see Fig. 3d). The low energy barrier in the two 2-Ortho carbon site is due to higher π electron occupancy of these C atoms, which helps to bind BH_3 more strongly. This increased π occupancy is contributed by the electrons in the π orbital of the adjacent nitrogen atom (back donation), where the carbon atoms have more than half filled π orbital [39,40].

3.2.2. B_2H_6 splitting on h-BN surface

The barrier energies for B_2H_6 splitting on h-BN surface doped with C and O atoms are calculated. Unlike graphene, it is not necessary to identify the dopant sites in h-BN since the two BH_3 molecules bind irrespective of the arrangement of the dopant. We found that O-doped h-BN surface can act as a better catalyst for B_2H_6 splitting than C-doped h-BN. The barrier energies for B_2H_6 splitting on 3C and 2O-doped h-BN system are 1.61 eV and 0.94 eV (shown in Fig. 3b and c), respectively. In the case of 2O-doped h-BN, three of the six valence electrons of oxygen contribute to the bonding with surrounding boron atoms, forming a sigma bond. The remaining valence electrons and lone pair make the adjacent boron sites more reactive than the 3C-doped h-BN surface. The barrier energies for B_2H_6 splitting on H-atoms adsorbed 3C and 2O-doped h-BN systems, are 1.81 and 1.52 eV, respectively (see Fig. 3e and f). This increased barrier is mainly due to the stronger binding of the H-atom to the surface, which requires more energy to desorb the H-atom to possibly form BH_4. Relatively, 2O-doped h-BN is more efficient than 3C-doped h-BN for BH_3 production. All the values of B_2H_6 splitting on various surfaces are given in Table 2. For the doped h-BN, localized donor state is created near the Fermi level. The 2O-doped h-BN surface shows large density of state at the Fermi level, which causes a reduction in barrier for B_2H_6 splitting (see Figure S4 (h) and (i)). The bonding analysis between the surfaces and the molecule is given in the supplementary information (Fig. S4).

3.2.3. B_2H_6 splitting on metal organic framework

Next, we consider a third surface, metal organic framework (MOF5), to examine its effectiveness for B_2H_6 splitting. We study two different sites: (i) nitrogen atoms as binding sites in benzene dicarboxylate (BDC) linker of MOF5 where two of the C atoms on the opposite side of the benzene ring (referred to as 2 N doped) (see Fig. 1d) and (ii) oxygen atoms labelled 1 and 2 in Fig. 1d as binding sites on metal-oxide cluster

Table 2
Barrier energies of B_2H_6 splitting on various surfaces.

Barrier energy for B_2H_6 splitting			
System	Site	E_A - Forward (eV)	E_A - Backward (eV)
4N-doped graphene	Carbon	0.74	0.51
3C-doped h-BN	Carbon	1.61	2.62
2O-doped h-BN	Boron	0.94	2.00
3N-doped graphene	Nitrogen	2.15	0.22
H adsorbed on 3N-doped graphene	Hydrogen	1.74	0.18
H adsorbed on 3C-doped h-BN	Hydrogen	1.81	0.24
H adsorbed on 2O-doped h-BN	Hydrogen	1.52	1.36
TiN(001) [23]	Nitrogen	1.11	–

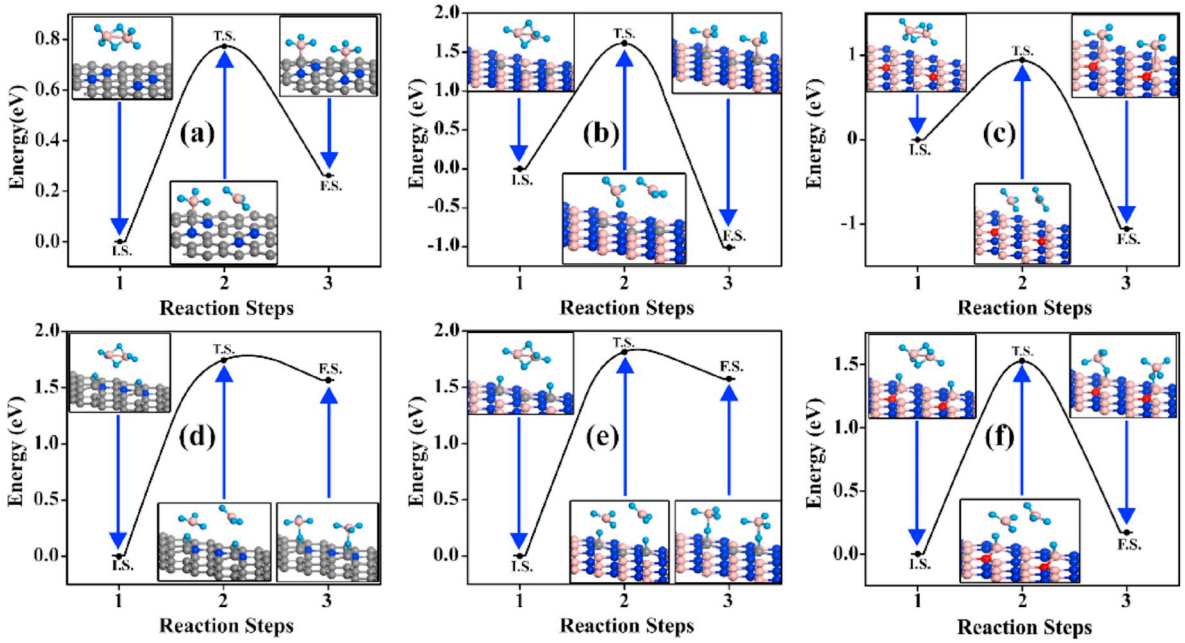

Fig. 3. Barrier energy for B_2H_6 splitting on (a) 4N-doped Graphene, (b) 3C-doped h-BN and (c) 2O-doped h-BN without adsorbed hydrogen atom. Barrier energy for B_2H_6 splitting on (d) 3N-doped Graphene, (e) 3C-doped h-BN and (f) 2O-doped h-BN with adsorbed hydrogen atom. I.S., T.S. and F.S. indicate the initial, transition and final state respectively. Insets show the initial, transition and final state structures. (Black line is to guide the eye.)

in un-doped MOF5. Note that in the case of pure MOF5, the BDC linker is unlikely to capture two BH_3 molecules ($2BH_3$) as it has a lower binding energy, namely −0.35 eV compared to −0.62 eV on 2 N doped BDC linker. Doping on the BDC linker does not influence binding on metal oxide cluster which is evident from the $2BH_3$ binding energies on metal oxide of −1.46 eV on undoped MOF5 and -1.47 eV on 2 N doped MOF5. For nitrogen atoms as binding site for 2 N doped MOF5, it requires 1.98 eV to dissociate a B_2H_6 molecule into two BH_3 molecules (Fig. 4a). For the second case, the barrier energy for B_2H_6 splitting is reduced to 1.36 eV (Fig. 4b). The possibility to reduce the barrier energy for splitting is further tested with replacing one Zn atom in the metal oxide cluster with Co and Fe atom. Botas et al. synthesized Co doped MOF5 which shows good gas (H_2, CH_4 and CO_2) adsorption behavior [41]. Also, the band gap of MOF5 can be tuned towards metallicity by varying the concentrations of the substituted Co atoms [42]. In another work, Brozek et al. have synthesized MOF5 with various metal ions replacing Zn atom and have shown that Fe-MOF5 activates NO more efficiently [43]. One Zn atom is replaced with Co atom and Fe atom on the metal cluster. In the case of Co-doped MOF5 the barrier energy for B_2H_6 splitting is 1.38 eV (Fig. 4c) and for Fe-doped MOF5, the barrier energy is 1.34 eV (Fig. 4d). Though the change in barrier energy is low in magnitude before and after doping, the type and concentration of dopants can be varied and is open to exploitation in reducing the B_2H_6 splitting energy.

3.3. Splitting of H_2 on BH_3 anchored to dopant sites in graphene

We now consider the splitting of H_2 molecule in the presence of BH_3 secondary catalyst. For this we focus on the 4N-doped graphene surface where one BH_3 molecule is adsorbed on 2-Ortho carbon site as model structure (see inset Fig. 5a). To estimate the barrier energy, we place the H_2 molecule at ~2 Å above the surface as the initial step. In the final step we consider the two hydrogen atoms adsorbed on 1-Ortho_1-Para and 2-Ortho carbon sites (see inset of Fig. 5a and b). The energy to split isolated H_2 molecule is 4.5 eV [44] experimentally while it is 2.62 eV on pristine graphene [45]. However, on 4 N doped graphene this energy is reduced to 1.13 eV. In the presence of adsorbed BH_3, the corresponding energy is 1.70 eV. So, nitrogen doped graphene surface can help to split both B_2H_6 and H_2 (even in the presence of BH_3). Relatively higher energy for H_2 splitting in the presence of adsorbed BH_3 is due to the reduction of charge distributed on the 1-Ortho_1-Para carbon by nitrogen dopant atom in the presence of adsorbed BH_3.

3.3.1. Splitting of H_2 on BH_3 anchored to dopant sites in h-BN and undoped MOF5

We then study H_2 splitting in the presence of BH_3 adsorbed on 3C-doped h-BN, O-doped h-BN and on undoped BDC linker of MOF5. BH_3 is placed on carbon dopant at the end and sites for 2H are, carbon in middle and boron atom (Fig. 5c). In this case, the barrier energy to split H_2 is 0.15 eV and in absence of adsorbed BH_3 the barrier energy is 0.25 eV (Fig. 5d). This shows that presence of BH_3 can reduce the barrier energy in splitting H_2. Even without adsorbed BH_3 the surface (3C-doped h-BN) itself is efficient in reducing the H_2 splitting energy from 4.5 eV to 0.25 eV. Finally, on MOF5, BH_3 is adsorbed on one side of BDC linker while 2H are adsorbed on the opposite side (Fig. 5e). The barrier energy in presence of BH_3 is 1.48 eV and the corresponding energy without BH_3 is 0.97 eV (Fig. 5f). The increased barrier energy with adsorbed BH_3 could be attributed to reduced charge on C atoms due to the presence of BH_3. 0.97 eV of barrier energy shows that BDC linker can split H_2 molecule effectively.

3.4. Generalization of the bond-exchange mechanism

Our final step is to study the migration of H once the H_2 is split. To generalize the bond-exchange mechanism, we focus on the migration of H-atoms on pure and N-doped graphene. First, we calculate the energy barrier for hydrogen atom migration on graphene surface without the aid of secondary catalyst. On pure graphene, the migration path is from one C site to the next site and in N-doped graphene, the path is from the site adjacent to the dopant to the next site. The energy barriers are given in Fig. 6 (a) and (c), which are 1.02 and 1.45 eV for pure and N-doped graphene, respectively. To facilitate final step of the spillover process, we need to reduce this energy barrier. Next, we consider BH_3 as the

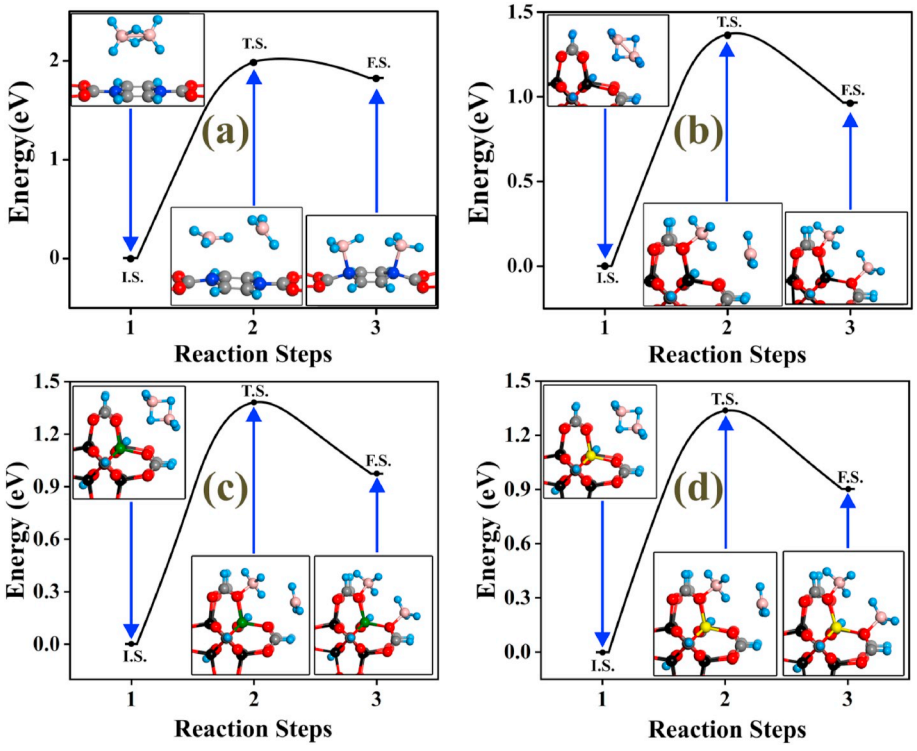

Fig. 4. Barrier energy for B_2H_6 splitting on (a) 2N-doped BDC linker (MOF5) on (b) Metal-oxide cluster (MOF5) on (c) Co doped Metal-oxide cluster (MOF5) and on (d) Fe doped Metal-oxide cluster (MOF5). I.S., T.S. and F.S. indicate the initial, transition and final state respectively. Insets show the initial, transition and final state structures. Green and yellow spheres represent Co and Fe atoms respectively. (Black line is to guide the eye only.). (For interpretation of the references to color in this figure legend, the reader is referred to the Web version of this article.)

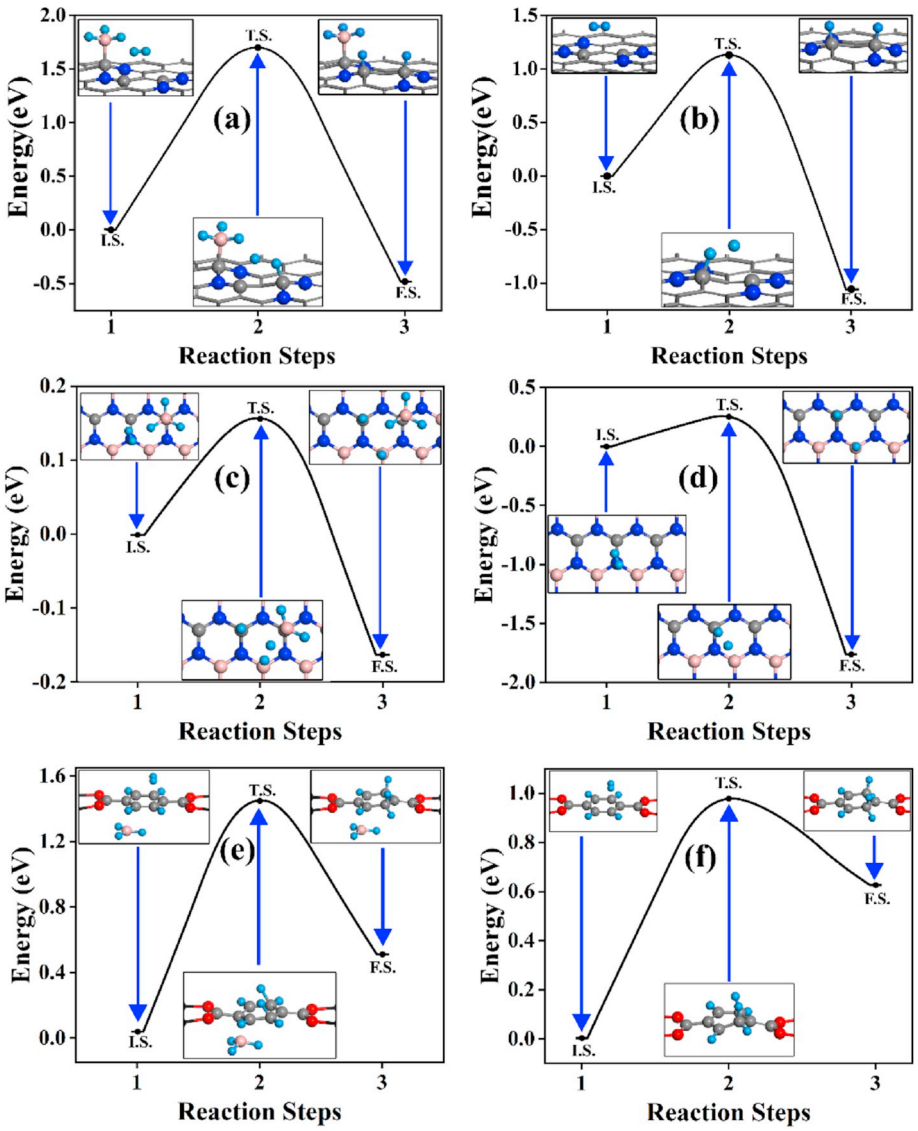

Fig. 5. Barrier energy for H_2 splitting on 4N-doped graphene (a) in presence of adsorbed BH_3, (b) without adsorbed BH_3; on 3C-doped h-BN (c) in presence of adsorbed BH_3, (d) without adsorbed BH_3; on undoped BDC linker of MOF5 (e) in presence of adsorbed BH_3 and (f) without adsorbed BH_3. I.S., T.S. and F.S. indicate the initial, transition and final state respectively. Insets show the initial, transition and final state structures. (Black line is to guide the eye only).

secondary catalyst for hydrogen atom migration via bond-exchange mechanism. For pure and single N-doped graphene, the energy barrier is found to be 0.21 eV and 0.07 eV, respectively (shown in Fig. 6 (b) and (d)).

The probability of BH_3 as secondary catalyst for facilitating the hydrogen atom migration is also studied in MOF5. In general, hydrogen uptake efficiency of MOF5, following spillover mechanism, is facilitated by the presence of metals such as Pt and Pd [46–49]. The energy barrier for H migration on the un-doped BDC linker is 1.4 eV without the aid of the secondary catalyst (Fig. 6e), which is reduced to 0.5 eV when BH_3 is used as a secondary catalyst by bond-exchange mechanism (Fig. 6f). These results confirm the importance of BH_3 as a secondary catalyst to lower the H-atom migration barrier.

4. Conclusion

In summary, we have studied symmetrical splitting of B_2H_6 on N-doped graphene, C and O-doped h-BN surface, and MOF5. We have shown that the resulting reduction in the energy barrier would facilitate the production of BH_3 as a secondary catalyst, and, hence, hydrogen sorption following the spillover mechanism. A structural descriptor based predictive model equation is developed to help screen active dopant sites for symmetrical splitting of B_2H_6. The validity of this model equation is established by comparing the predicted energies with those based on explicit DFT-based calculations. We show that B_2H_6 can be efficiently split on N-doped graphene, C and O-doped h-BN and MOF5. The lowest energy barrier for the B_2H_6 splitting is 0.77 eV for 4N-doped graphene. We have studied the role, BH_3 molecule plays in splitting H_2 molecule on all the surfaces and all surfaces are effective in reducing the inherent high H_2 splitting energy of 4.5 eV. We also studied the migration of the H atom through bond-exchange mechanism on graphene surfaces. The energy barrier for H migration, namely, 1.02 eV and 1.45 eV are reduced to 0.21 eV and 0.07 eV when BH_3 is used as a secondary catalyst on pure and N-doped graphene, respectively. In the case of MOF5, the metal-oxide cluster is more efficient than the BDC linker for splitting B_2H_6. Overall, the structural catalytic descriptor, predictive model equation and the symmetrical splitting of B_2H_6 can address the reversible hydrogen storage problem through the spillover mechanism.

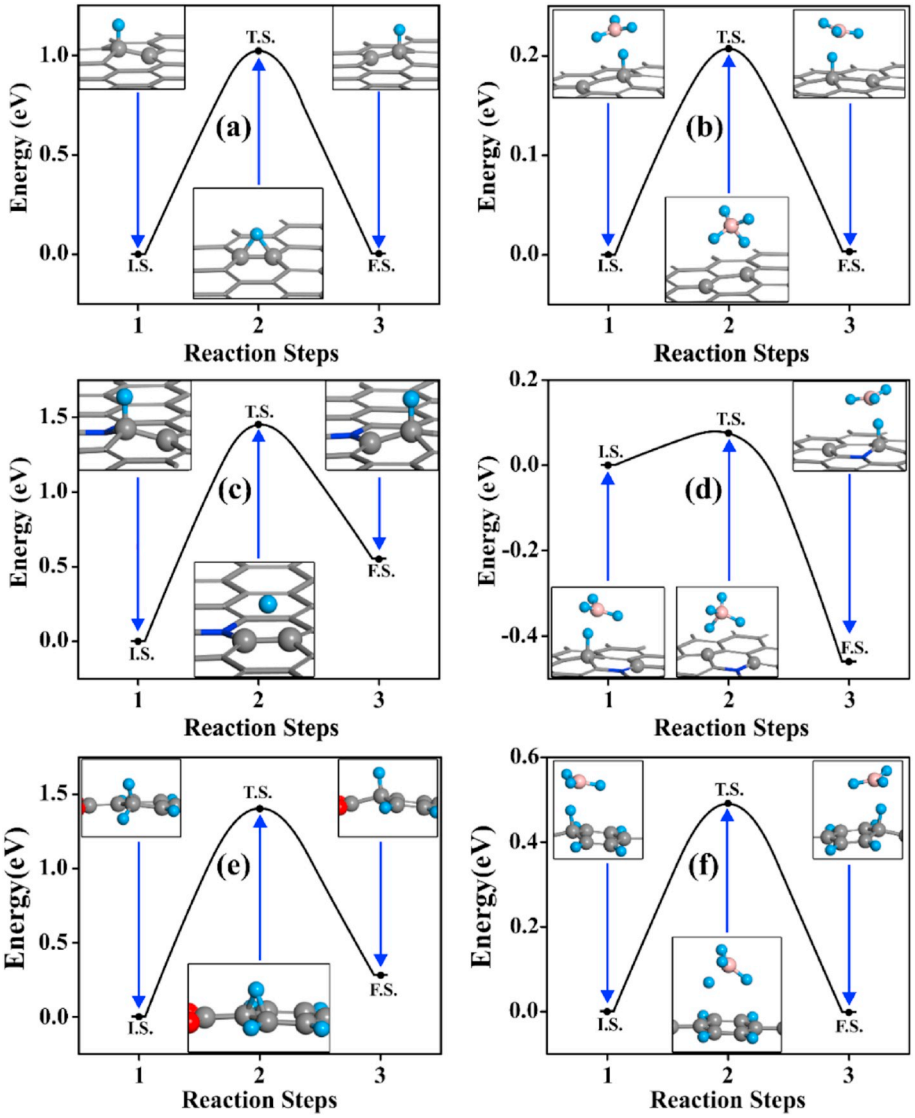

Fig. 6. Migration barrier energy of single H-atom on (a) Pure and (c) N-doped graphene without secondary catalyst and (b) & (d) using BH_3 as secondary catalyst through bond exchange mechanism. Barrier energy for H-atom migration on undoped BDC linker on MOF5 without secondary catalyst (e) and (f) H-atom migration using BH_3 as secondary catalyst by bond-exchange mechanism. I.S., T.S. and F.S. indicate the initial, transition and final state respectively. Insets show the initial, transition and final state structures. (Black line is guide to the eye).

Declaration of competing interest

The authors declare that they have no known competing financial interests or personal relationships that could have appeared to influence the work reported in this paper.

Acknowledgement

R.T. thanks Science and Engineering Research Board (SERB), India, for the financial support (Grant Nos. EMR/2016/004689). E.S.E. and R. T. thanks Board of Research in Nuclear Sciences (BRNS), India, for the financial support (Grant Nos. 37(2)/20/14/2018-BRNS/37144). Authors thank High Performance Computing Center, SRM IST for providing the computational facility. PJ acknowledges partial supported from the U.S. Department of Energy, Office of Basic Energy Sciences, Division of Materials Sciences and Engineering under Award No.DE-FG02-96ER45579.

Appendix A. Supplementary data

Supplementary data to this article can be found online at https://doi.org/10.1016/j.jpowsour.2020.227973.

References

[1] P. Jena, Materials for hydrogen storage: past, present, and future, J. Phys. Chem. Lett. 2 (2011) 206–211, https://doi.org/10.1021/jz1015372.
[2] R. Prins, Hydrogen spillover. Facts and fiction, Chem. Rev. 112 (2012) 2714–2738, https://doi.org/10.1021/cr200346z.
[3] M. Blanco-Rey, J.I. Juaristi, M. Alducin, M.J. López, J.A. Alonso, Is spillover relevant for hydrogen adsorption and storage in porous carbons doped with palladium nanoparticles? J. Phys. Chem. C 120 (2016) 17357–17364, https://doi.org/10.1021/acs.jpcc.6b04006.
[4] C.S. Tsao, Y.R. Tzeng, M.S. Yu, C.Y. Wang, H.H. Tseng, T.Y. Chung, H.C. Wu, T. Yamamoto, K. Kaneko, S.H. Chen, Effect of catalyst size on hydrogen storage capacity of Pt-impregnated active carbon via spillover, J. Phys. Chem. Lett. 1 (2010) 1060–1063, https://doi.org/10.1021/jz100149u.
[5] E. Ruse, S. Pevzner, I. Pri Bar, R. Nadiv, V.M. Skripnyuk, E. Rabkin, O. Regev, Hydrogen storage and spillover kinetics in carbon nanotube-Mg composites, Int. J. Hydrogen Energy 41 (2016) 2814–2819, https://doi.org/10.1016/j.ijhydene.2015.12.017.
[6] H. Nishihara, T. Simura, T. Kyotani, Enhanced hydrogen spillover to fullerene at ambient temperature, Chem. Commun. 54 (2018) 3327–3330, https://doi.org/10.1039/c8cc00265g.
[7] V.B. Parambhath, R. Nagar, S. Ramaprabhu, Effect of nitrogen doping on hydrogen storage capacity of palladium decorated graphene, Langmuir 28 (2012) 7826–7833, https://doi.org/10.1021/la301232r.
[8] H. Cheng, L. Chen, A.C. Cooper, X. Sha, G.P. Pez, Hydrogen spillover in the context of hydrogen storage using solid-state materials, Energy Environ. Sci. 1 (2008) 338, https://doi.org/10.1039/b807618a.
[9] T.Y. Chung, C.S. Tsao, H.P. Tseng, C.H. Chen, M.S. Yu, Effects of oxygen functional groups on the enhancement of the hydrogen spillover of Pd-doped activated

carbon, J. Colloid Interface Sci. 441 (2015) 98–105, https://doi.org/10.1016/j.jcis.2014.10.062.
[10] H.L. Tierney, A.E. Baber, J.R. Kitchin, E.C.H. Sykes, Hydrogen dissociation and spillover on individual isolated palladium atoms, Phys. Rev. Lett. 103 (2009) 1–4, https://doi.org/10.1103/PhysRevLett.103.246102.
[11] G.P. Das, A. Bhattacharya, S. Bhattacharya, C. Majumder, Transition-metal decoration enhanced room-temperature hydrogen storage in a defect-modulated graphene sheet, J. Phys. Chem. C 114 (2010) 10297–10301, https://doi.org/10.1021/jp100230c.
[12] S.H. Mushrif, A.D. Rey, G.H. Peslherbe, Energetics and dynamics of hydrogen adsorption, desorption and migration on a carbon-supported palladium cluster, J. Mater. Chem. 20 (2010) 10503–10510, https://doi.org/10.1039/c0jm01559h.
[13] S.S. Han, H. Jung, D.H. Jung, S.H. Choi, N. Park, Stability of hydrogenation states of graphene and conditions for hydrogen spillover, Phys. Rev. B Condens. Matter 85 (2012) 155408, https://doi.org/10.1103/PhysRevB.85.155408.
[14] Y. Zhao, T. Gennett, Water-mediated cooperative migration of chemisorbed hydrogen on graphene, Phys. Rev. Lett. 112 (2014) 1–5, https://doi.org/10.1103/PhysRevLett.112.076101.
[15] R. Campesi, F. Cuevas, M. Latroche, M. Hirscher, Hydrogen spillover measurements of unbridged and bridged metal-organic frameworks - Revisited, Phys. Chem. Chem. Phys. 12 (2010) 10457–10459, https://doi.org/10.1039/c0cp00037j.
[16] S.M. Luzan, A.V. Talyzin, Hydrogen adsorption in Pt catalyst/MOF-5 materials, Microporous Mesoporous Mater. 135 (2010) 201–205, https://doi.org/10.1016/j.micromeso.2010.07.018.
[17] Y. Li, F.H. Yang, R.T. Yang, Kinetics and mechanistic model for hydrogen spillover on bridged metal - organic frameworks, J. Phys. Chem. C 111 (2007) 3405–3411, https://doi.org/10.1021/jp065367q.
[18] K. Lee, Y.H. Kim, Y.Y. Sun, D. West, Y. Zhao, Z. Chen, S.B. Zhang, Hole-mediated hydrogen spillover mechanism in metal-organic frameworks, Phys. Rev. Lett. 104 (2010) 1–4, https://doi.org/10.1103/PhysRevLett.104.236101.
[19] Y. Li, R.T. Yang, Hydrogen storage in metal-organic frameworks by bridged hydrogen spillover, J. Am. Chem. Soc. 128 (2006) 8136–8137, https://doi.org/10.1021/ja061681m.
[20] S.S. Han, H. Kim, N. Park, Effect of shuttling catalyst on the migration of hydrogen adatoms: a strategy for the facile hydrogenation of graphene, J. Phys. Chem. C 115 (2011) 24696–24701.
[21] E.M. Kumar, S. Sinthika, R. Thapa, First principles guide to tune h-BN nanostructures as superior light-element-based hydrogen storage materials: role of the bond exchange spillover mechanism, J. Mater. Chem. A. 3 (2015) 304–313.
[22] E.M. Kumar, B. Prajapat, B. Saha, R. Thapa, Spillover of hydrogen on SiC-ML surface: doping effect and bond exchange mechanism, Int. J. Hydrogen Energy 41 (2016) 3928–3939.
[23] H. Park, S. Lee, H.J. Kim, E. Yoon, G.-D. Lee, Dissociation reaction of B_2H_6 on TiN surfaces during atomic layer deposition: first-principles study, RSC Adv. 7 (2017) 55750–55755, https://doi.org/10.1039/C7RA11291B.
[24] O. Friedrichs, A. Remhof, A. Borgschulte, F. Buchter, S.I. Orimo, A. Züttel, Breaking the passivation - the road to a solvent free borohydride synthesis, Phys. Chem. Chem. Phys. 12 (2010) 10919–10922, https://doi.org/10.1039/c0cp00022a.
[25] R.W. Parry, Symmetric and asymmetric cleavage of the lighter boron hydrides and of metal salts - the role of the dielectric constant, J. Organomet. Chem. (2000) 614–615, https://doi.org/10.1016/S0022-328X(00)00591-X, 5–9.
[26] S. Sakai, Ab initio molecular orbital study of the chemical reactions of diborane with ammonia, J. Phys. Chem. 99 (1995) 5883–5888, https://doi.org/10.1021/j100016a023.
[27] M.L. McKee, Ab initio study of the formation of H2B=NH2 from NH3 and B2H6, J. Phys. Chem. 96 (1992) 5380–5385.
[28] E. Mayer, Symmetrical cleavage of diborane by ammonia in solution, Inorg. Chem. 11 (1972) 866–869, https://doi.org/10.1021/ic50110a044.
[29] V.S. Nguyen, M.H. Matus, M.T. Nguyen, D.A. Dixon, Reactions of diborane with ammonia and ammonia borane: catalytic effects for multiple pathways for hydrogen release, J. Phys. Chem. 112 (2008) 9946–9954, https://doi.org/10.1021/jp804714r.
[30] G. Kresse, J. Furthmüller, Efficiency of ab-initio total energy calculations for metals and semiconductors using a plane-wave basis set, Comput. Mater. Sci. 6 (1996) 15–50.
[31] J.P. Perdew, K. Burke, M. Ernzerhof, Generalized gradient approximation made simple, Phys. Rev. Lett. 77 (1996) 3865.
[32] P.E. Blöchl, Projector augmented-wave method, Phys. Rev. B 50 (1994) 17953.
[33] W. Tang, E. Sanville, G. Henkelman, A grid-based Bader analysis algorithm without lattice bias, J. Phys. Condens. Matter 21 (2009) 84204.
[34] G. Henkelman, B.P. Uberuaga, H. Jónsson, A climbing image nudged elastic band method for finding saddle points and minimum energy paths, J. Chem. Phys. 113 (2000) 9901–9904.
[35] Z. Bo, X. Guo, X. Wei, H. Yang, J. Yan, K. Cen, Mutualistic decomposition pathway of formaldehyde on O-predosed δ-MnO2, Appl. Surf. Sci. 498 (2019) 143784, https://doi.org/10.1016/j.apsusc.2019.143784.
[36] L.H. Long, The mechanisms of thermal decomposition of diborane and of interconversion of the boranes: a reinterpretation of the evidence, J. Inorg. Nucl. Chem. 32 (1970) 1097–1115.
[37] K. Kawaguchi, J.E. Butler, C. Yamada, S.H. Bauer, T. Minowa, H. Kanamori, E. Hirota, Observation of the gas-phase infrared spectrum of BH3, J. Chem. Phys. 87 (1987) 2438–2441, https://doi.org/10.1063/1.453135.
[38] H. Zhang, G. Xia, J. Zhang, D. Sun, Z. Guo, X. Yu, Graphene-tailored thermodynamics and kinetics to fabricate metal borohydride nanoparticles with high purity and enhanced reversibility, Adv. Energy Mater. 8 (2018) 1–9, https://doi.org/10.1002/aenm.201702975.
[39] S. Sinthika, U.V. Waghmare, R. Thapa, Structural and electronic descriptors of catalytic activity of graphene-based materials: first-principles theoretical analysis, Small 14 (2018) 1–10, https://doi.org/10.1002/smll.201703609.
[40] S. Sinthika, R. Thapa, Influence of enolate/epoxy configuration, doping and vacancy on the catalytic activity of graphene, RSC Adv. 5 (2015) 93215–93225, https://doi.org/10.1039/c5ra20127f.
[41] J.A. Botas, G. Calleja, M. Sánchez-Sánchez, M.G. Orcajo, Cobalt doping of the MOF-5 framework and its effect on gas-adsorption properties, Langmuir 26 (2010) 5300–5303, https://doi.org/10.1021/la100423a.
[42] J.H. Choi, Y.J. Choi, J.W. Lee, W.H. Shin, J.K. Kang, Tunability of electronic band gaps from semiconducting to metallic states via tailoring Zn ions in MOFs with Co ions, Phys. Chem. Chem. Phys. 11 (2009) 628–631, https://doi.org/10.1039/b816668d.
[43] C.K. Brozek, M. Dincă, Ti3+-, V2+/3+-, Cr2+/3+-, Mn 2+-, and Fe2+-substituted MOF-5 and redox reactivity in Cr- and Fe-MOF-5, J. Am. Chem. Soc. 135 (2013) 12886–12891, https://doi.org/10.1021/ja4064475.
[44] A. Balakrishnan, V. Smith, B.P. Stoicheff, Dissociation energies of the hydrogen and deuterium molecules, Phys. Rev. 49 (1994) 2460–2469, https://doi.org/10.1103/PhysRevA.49.2460.
[45] F. Costanzo, P.L. Silvestrelli, F. Ancilotto, Physisorption, diffusion, and chemisorption pathways of H2 molecule on graphene and on (2,2) carbon nanotube by first principles calculations, J. Chem. Theor. Comput. 8 (2012) 1288–1294, https://doi.org/10.1021/ct300143a.
[46] H. Zhou, J. Zhang, J. Zhang, X.F. Yan, X.P. Shen, A.H. Yuan, Spillover enhanced hydrogen storage in Pt-doped MOF/graphene oxide composite produced via an impregnation method, Inorg. Chem. Commun. 54 (2015) 54–56, https://doi.org/10.1016/j.inoche.2015.02.001.
[47] N.R. Stuckert, L. Wang, R.T. Yang, Characteristics of hydrogen storage by spillover on Pt-doped carbon and catalyst-bridged metal organic framework, Langmuir 26 (2010) 11963–11971, https://doi.org/10.1021/la101377u.
[48] C. Zlotea, R. Campesi, F. Cuevas, E. Leroy, P. Dibandjo, C. Volkringer, T. Loiseau, G. Férey, M. Latroche, Pd nanoparticles embedded into a metal-organic framework: synthesis, structural characteristics, and hydrogen sorption properties, J. Am. Chem. Soc. 132 (2010) 2991–2997, https://doi.org/10.1021/ja9084995.
[49] T. Wang, Q. Zhang, B. Li, H. Chen, L. Chen, Density functional study of hydrogen spillover on direct Pd-doped metal-organic frameworks IRMOF-1, Int. J. Hydrogen Energy 37 (2012) 5081–5089, https://doi.org/10.1016/j.ijhydene.2011.12.065.